Journal of Magnetic Resonance **141,** 121–132 (1999)
Article ID jmre.1999.1867, available online at http://www.idealibrary.com on IDEAL®

Line Narrowing of $I = \frac{1}{2}$ Spins Coupled to Quadrupolar Nuclei in Liquids: Effects of Weak Decoupling Fields

P. Bendel* and A. Baram†

**Department of Chemical Services, MR Center, The Weizmann Institute of Science, Rehovot 76100, Israel; and †Soreq NRC, Yavne 81800, Israel*

Received March 17, 1999; revised June 23, 1999

In this paper an exact description of the observed transverse magnetization of spin $\frac{1}{2}$ nuclei, coupled to quadrupolar spins which are subjected to RF irradiation, is presented. It is shown that for on-resonance CW decoupling at weak to intermediate irradiation levels, the transverse decay of the spin $\frac{1}{2}$ magnetization is modulated with a period of $1/\nu_2$, where ν_2 is the amplitude of the decoupling irradiation. When the spin $\frac{1}{2}$ signal is created as a spin echo, and the quadrupolar resonance continuously irradiated during the echo evolution, the echo amplitudes experience much stronger modulation with period $2/\nu_2$. In previous treatments of such spin systems, the regime of weak decoupling power was usually neglected, and approximate analytical expressions seeking to define the "adequate" or "minimal" decoupling power, necessary to achieve the collapse of the spin $\frac{1}{2}$ multiplet into a single narrow line, were derived. It is demonstrated here, both by experiments and by simulations using a full Redfield formalism, that simple analytical predictions for the T_2 decay of the spin $\frac{1}{2}$ magnetization are still possible, even when the scalar relaxation is not in the "fast exchange" limit and the transverse decay is considerably modulated due to insufficient decoupling power. In this case, the expected single exponential decay rate is obtained for the nonmodulated component of the signal. The theoretical solution for spin $I = \frac{1}{2}$ coupled to $S = 3$ is derived, and results for the proton decay in ^{10}B-enriched sodium borocaptate in aqueous solution are presented. The effects of irradiation by several composite pulse decoupling sequences are also considered.

Key Words: **SEDOR; scalar relaxation; borocaptate sodium; ^{10}B inverse detection; decoupling.**

INTRODUCTION

The liquid-state lineshape (or transverse relaxation) of spin $I = \frac{1}{2}$ magnetization, with scalar coupling to a quadrupolar spin S, is usually affected both by the static effect of the coupling interaction and by its time-dependent modulation through the rapid spin–lattice relaxation of the quadrupolar spin (scalar relaxation of the second kind (*1*)). The analysis of such systems, in the presence of irradiation of the S spins, was presented in several publications, starting in the early days of CW NMR spectroscopy (*2*). Browne *et al.* (*3*) presented analytical equations for the calculation of $1/T_2^{sc}$, the residual scalar relaxation contribution to the transverse relaxation of spin I, in the presence of S-spin irradiation. More recently, Murali and Rao (*4*) published an extensive treatment of the ($I = \frac{1}{2}$; $S = 1$) spin system, paying particular attention to cross-relaxation effects, which may be expected for ^{13}C–^{2}H moieties in peptides and proteins. Skrynnikov *et al.* (*5*) extended the analysis to situations where both the I and S spins are irradiated simultaneously, revealing interesting effects of enhancement of $T_{1\rho}$ relaxation. However, the phenomenon of strong cyclic modulation caused by the decoupling was not described in such systems, to the best of our knowledge.

There is, of course, a vast amount of literature covering decoupling in ($I = \frac{1}{2}/S = \frac{1}{2}$) spin systems. Cyclic effects, leading to "coherence sidebands" in the frequency domain, received some recent attention in the context of adiabatic decoupling (*6, 7*) and decoupling by composite pulse sequences (*8*). Coherent, on-resonance CW decoupling was also predicted to lead to the appearance of sidebands (*9–11*). Freeman and Hill (*12*) noticed the periodic effect of decoupling on the apparent T_2 values measured by Hahn spin-echo pulse sequences. The effect of scalar relaxation was usually ignored in such spin $\frac{1}{2}$ systems, but must be taken into account when S is a quadrupolar spin.

The recent interest in the exact effects of S-spin irradiation on I-spin lineshapes and linewidths is mainly motivated by the increasingly popular practice of conducting high-resolution multidimensional NMR experiments on deuterated proteins, using ^{2}H decoupling to narrow the signals of adjacent ^{13}C, ^{15}N, or proton resonances. Our own interest stems from a somewhat different motivation, namely the possibility for indirect detection of low-sensitivity quadrupolar spins, such as ^{10}B (spin $S = 3$), via protons exhibiting a scalar ^{1}H–^{10}B coupling interaction (*13, 14*). Pulse sequences for such indirect detection, in particular sequences which also achieve spatial resolution of some form, will usually be based on spin-echo detection, and selectively applied S-spin irradiation (combined with appropriate phase cycling) can be the basis for selectively detecting only the protons coupled to the S spins (*15*). Such pulse sequences can usually be classified as spin-echo double-resonance (SEDOR) experiments (*16*). Therefore, we were mainly interested in characterizing the time-domain evolution of the

1090-7807/99 $30.00

TABLE 1
Diagonal Elements of Matrix A

k	m_S, m'_S	A_{kk}	k	m_S, m'_S	A_{kk}
1	3, 3	$i3J' - 75j_1 - 30j_2$	15	1, 2	$i(\Delta\omega_S + \frac{3}{2}J') - \frac{27}{2}j_0 - \frac{171}{2}j_1 - 81j_2$
2	2, 2	$i2J' - 120j_1 - 60j_2$	16	0, 1	$i(\Delta\omega_S + \frac{1}{2}J') - \frac{3}{2}j_0 - \frac{63}{2}j_1 - 111j_2$
3	1, 1	$iJ' - 51j_1 - 102j_2$	17	−1, 0	$i(\Delta\omega_S - \frac{1}{2}J') - \frac{3}{2}j_0 - \frac{63}{2}j_1 - 111j_2$
4	0, 0	$-12j_1 - 120j_2$	18	−2, −1	$i(\Delta\omega_S - \frac{3}{2}J') - \frac{27}{2}j_0 - \frac{171}{2}j_1 - 81j_2$
5	−1, −1	$-iJ' - 51j_1 - 102j_2$	19	−3, −2	$i(\Delta\omega_S - \frac{5}{2}J') - \frac{75}{2}j_0 - \frac{195}{2}j_1 - 45j_2$
6	−2, −2	$-i2J' - 120j_1 - 60j_2$	20	3, 1	$i(-2\Delta\omega_S + 2J') - 96j_0 - 63j_1 - 66j_2$
7	−3, −3	$-i3J' - 75j_1 - 30j_2$	21	2, 0	$i(-2\Delta\omega_S + J') - 24j_0 - 66j_1 - 90j_2$
8	3, 2	$i(-\Delta\omega_S + \frac{5}{2}J') - \frac{75}{2}j_0 - \frac{195}{2}j_1 - 45j_2$	22	1, −1	$i(-2\Delta\omega_S) - 51j_1 - 102j_2$
9	2, 1	$i(-\Delta\omega_S + \frac{3}{2}J') - \frac{27}{2}j_0 - \frac{171}{2}j_1 - 81j_2$	23	0, −2	$i(-2\Delta\omega_S - J') - 24j_0 - 66j_1 - 90j_2$
10	1, 0	$i(-\Delta\omega_S + \frac{1}{2}J') - \frac{3}{2}j_0 - \frac{63}{2}j_1 - 111j_2$	24	−1, −3	$i(-2\Delta\omega_S - 2J') - 96j_0 - 63j_1 - 66j_2$
11	0, −1	$i(-\Delta\omega_S - \frac{1}{2}J') - \frac{3}{2}j_0 - \frac{63}{2}j_1 - 111j_2$	25	1, 3	$i(2\Delta\omega_S + 2J') - 96j_0 - 63j_1 - 66j_2$
12	−1, −2	$i(-\Delta\omega_S - \frac{3}{2}J') - \frac{27}{2}j_0 - \frac{171}{2}j_1 - 81j_2$	26	0, 2	$i(2\Delta\omega_S + J') - 24j_0 - 66j_1 - 90j_2$
13	−2, −3	$i(-\Delta\omega_S - \frac{5}{2}J') - \frac{75}{2}j_0 - \frac{195}{2}j_1 - 45j_2$	27	−1, −3	$i(2\Delta\omega_S) - 51j_1 - 102j_2$
14	2, 3	$i(\Delta\omega_S + \frac{5}{2}J') - \frac{75}{2}j_0 - \frac{195}{2}j_1 - 45j_2$	28	−2, 0	$i(2\Delta\omega_S - J') - 24j_0 - 66j_1 - 90j_2$
			29	−3, −1	$i(2\Delta\omega_S - 2J') - 96j_0 - 63j_1 - 66j_2$

Note. The assignment of the various m_s and m'_S values to the indexes (k) of the matrix is, in principle, arbitrary. However, conventionally, the matrix is subdivided into blocks of different coherence order, $\Delta m_S = 0$ (k = 1–7), $\Delta m_S = \pm 1$ (k = 8–19), and $\Delta m_S = \pm 2$ (k = 20–29). For all the coherences listed in this table, $m_I = \frac{1}{2}$ and $m'_I = -\frac{1}{2}$. Therefore, all diagonal terms should also include the quantity $i(-\Delta\omega_I)$, i.e., the rotating-frame resonance offset of the I spins, which can be set to 0 without loss of generality, and which, experimentally, does not affect the evolution of the magnetization, if spin echoes are detected. As indicated in the text, a parameter, $-r_2$, can be added to the diagonal terms to account for independent transverse relaxation of the I spins. $J' = 2\pi J$.

^{1}H spin echo, as function of the S-spin decoupling power, including the case of no irradiation, which was also addressed in a previous publication (*17*). The consideration of weak decoupling power is very important from a practical point of view: in medical MRI practice, the RF coils are large, S-spin resonance frequencies will be very low, and irradiation power levels must be limited due to safety considerations for the patient.

The problem of proton-detected spectroscopy (or imaging) of a low-sensitivity quadrupolar spin, using S-spin decoupling, also arises for the indirect detection of ^{17}O (*18*, *19*), although in this case the interaction is also modulated by chemical exchange of the protons from the ^{17}O-labeled molecules, a complication which is not considered in the present contribution.

Here we derive the time-dependent evolution of $I = \frac{1}{2}$ spin magnetization, coupled to an $S = 3$ nucleus, in the presence of S-spin irradiation, following the approach used by Murali and Rao (*4*). Only the quadrupolar relaxation mechanism is considered for S, and cross-relaxation effects are ignored, as these assumptions seemed to be justified for the system which was investigated experimentally. The sodium salt of mercaptoundecahydro-*closo*-dodecaborane, $Na_2B_{12}H_{12}S$ (BSH), enriched in ^{10}B, was dissolved either in deuterium oxide or in deuterated glycerol, to achieve a wider range of quadrupolar relaxation times, T_{1Q}. The echo-time-dependent intensity of the ^{10}B-coupled proton resonances was measured at different temperatures and ^{10}B irradiation power levels, and the results were shown to be in very good agreement with theoretical predictions.

THEORY

The energy level manifold for an $I = \frac{1}{2}$, S-spin pair contains $2(2S + 1)$ energy levels for all the possible combinations of m_I and m_S. Since we are ultimately interested in detectable I-spin magnetization, we consider all transitions for which $\Delta m_I = 1$ and $\Delta m_S = 0, \pm 1, \pm 2$. There are $10S - 1$ such transitions, which will be labeled by the indexes m_S and m'_S of the two connected energy levels. The time evolution of the magnetization can be found from solving

$$\frac{d\sigma}{dt} = -i[\mathbf{H}_0(t) + 2\pi J\mathbf{I}\cdot\mathbf{S} + \mathbf{H}^Q(t), \sigma], \qquad [1]$$

where

$$\mathbf{H}_0(t) = -[\omega_{oI}\mathbf{I}_z + \omega_{oS}\mathbf{S}_z] + \omega_2(\mathbf{S}_x\cos\omega_S t + \mathbf{S}_y\sin\omega_S t). \qquad [2]$$

ω_{oI} and ω_{oS} are the Larmor frequencies for I and S, respectively, ω_S is the frequency at which the S spins are irradiated, and ω_2 is the amplitude of this irradiation. J is the hetero-

TABLE 2
Off-Diagonal Elements of Matrix A

(k, l)	$A_{k,l}$	(k, l)	$A_{k,l}$
(1, 2) (6, 7)	$75j_1$	(21, 22) (22, 23) (26, 27) (27, 28)	$-3\sqrt{30}j_1$
(2, 3) (5, 6)	$45j_1$	(8, 10) (11, 13) (14, 16) (17, 19)	$30\sqrt{2}j_2$
(3, 4) (4, 5)	$6j_1$	(9, 11) (10, 12) (15, 17) (16, 18)	$12\sqrt{30}j_2$
(1, 3) (5, 7)	$30j_2$	(20, 22) (22, 24) (25, 27) (27, 29)	$12\sqrt{15}j_2$
(2, 4) (4, 6) (21, 25) (24, 28)	$60j_2$	(1, 8) (2, 14) (6, 13) (7, 19) (12, 24) (15, 25)	$i\frac{\sqrt{6}}{2}\omega_2$
(3, 5)	$72j_2$	(1, 14) (2, 8) (6, 19) (7, 13) (9, 25) (18, 29)	$-i\frac{\sqrt{6}}{2}\omega_2$
(8, 9) (12, 13) (14, 15) (18, 19)	$15\sqrt{15}j_1$	(2, 9) (3, 15) (5, 12) (6, 18) (8, 20) (16, 26) (11, 23) (19, 29)	$i\frac{\sqrt{10}}{2}\omega_2$
(9, 10) (11, 12) (15, 16) (17, 18)	$3\sqrt{30}j_1$	(2, 15) (3, 9) (5, 18) (6, 12) (14, 25) (10, 21) (17, 28) (13, 24)	$-i\frac{\sqrt{10}}{2}\omega_2$
(10, 11) (16, 17)	$-6j_1$	(3, 10) (4, 16) (4, 11) (5, 17) (9, 21) (10, 22) (17, 27) (18, 28)	$i\frac{\sqrt{12}}{2}\omega_2$
(20, 21) (23, 24) (25, 26) (28, 29)	$5\sqrt{18}j_1$	(3, 16) (4, 10) (4, 17) (5, 11) (15, 26) (16, 27) (11, 22) (12, 23)	$-i\frac{\sqrt{12}}{2}\omega_2$

Note. $A_{kl} = A_{lk}$, and $\omega_2 = 2\pi\nu_2$. All remaining off-diagonal elements are 0.

nuclear coupling constant, and $\mathbf{H}^Q(t)$ is the Hamiltonian for the quadrupolar relaxation. Equation [1] can be transformed into a doubly rotating frame in which $\mathbf{H}_0$ is time independent. In this frame,

$$\frac{d\sigma^*}{dt} = -i[\mathbf{H}^*, \sigma^*] - \Gamma(\sigma^* - \sigma_o), \qquad [3]$$

where Γ is the Redfield relaxation superoperator, and

$$\mathbf{H}^* = \mathbf{H}_z + \mathbf{H}_J + \mathbf{H}_x \qquad [4]$$

$$\mathbf{H}_z = -(\Delta\omega_I \mathbf{I}_z + \Delta\omega_S \mathbf{S}_z)$$

$$\mathbf{H}_J = 2\pi J \mathbf{I}_z \mathbf{S}_z$$

$$\mathbf{H}_x = \omega_2 \mathbf{S}_x. \qquad [5]$$

$\Delta\omega_I$ is the offset between the I-spin Larmor frequency and the reference receiver detection frequency, and $\Delta\omega_S$ is the difference between the S-spin Larmor frequency and the frequency for the S-spin irradiation. A formal solution to Eq. [3] is of the form

$$\sigma'(t) = e^{\mathbf{A}t}\sigma'(0), \qquad [6]$$

where σ' is the density matrix in the high-temperature approximation (*16*).

Immediately following a 90° proton pulse, the density matrix representing the proton spin magnetization, $\sigma'(0)$, will consist of a column vector with values of 1 for the elements representing the $2S + 1$ transitions for which $\Delta m_S = 0$ and with values of 0 for all the remaining elements.

The terms of the matrix **A** are given by

$$\begin{aligned} A_{kl} &= i\Big\{\delta_{kl}\Big[\Big\langle \frac{1}{2}, \alpha \Big| \mathbf{H}_z + \mathbf{H}_J \Big| \frac{1}{2}, \alpha \Big\rangle - \Big\langle -\frac{1}{2}, \alpha' \Big| \mathbf{H}_z \\ &\quad + \mathbf{H}_J \Big| -\frac{1}{2}, \alpha' \Big\rangle\Big] + \delta_{\alpha\beta}\Big\langle -\frac{1}{2}, \alpha' \Big| \mathbf{H}_x \Big| -\frac{1}{2}, \beta' \Big\rangle \\ &\quad - \delta_{\alpha'\beta'}\Big\langle -\frac{1}{2}, \alpha \Big| \mathbf{H}_x \Big| -\frac{1}{2}, \beta \Big\rangle\Big\} + R_{\alpha\alpha'\beta\beta'} \\ &= i\Big\{\delta_{kl}\Big[\frac{J}{2}(\alpha + \alpha') - \Delta\omega_I + (\alpha' - \alpha)\Delta\omega_S\Big] \\ &\quad + \omega_2(\delta_{\alpha\beta}\langle\alpha'|\mathbf{S}_x|\beta'\rangle - \delta_{\alpha'\beta'}\langle\alpha|\mathbf{S}_x|\beta\rangle)\Big\} \\ &\quad + R_{\alpha\alpha'\beta\beta'}, \end{aligned} \qquad [7]$$

where $\alpha = m_S(k)$, $\alpha' = m'_S(k)$, $\beta = m_S(l)$, and $\beta' = m'_S(l)$. The assignment of the indexes k and l to the different values of

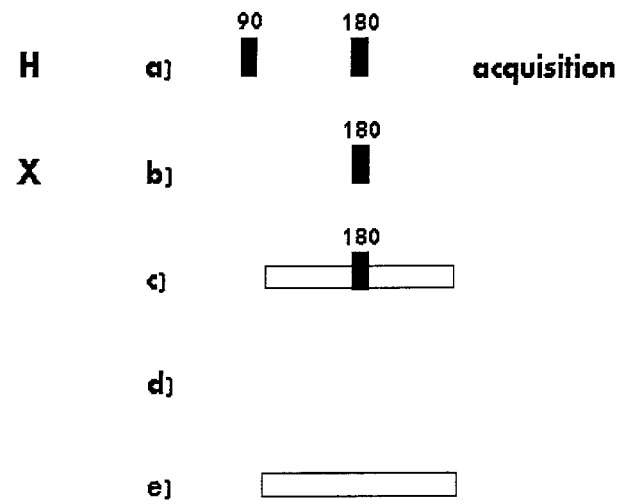

FIG. 1. Schematic diagram of the different SEDOR pulse sequences applied to obtain the results in this study. In all experiments, sequence a was applied to the ^{1}H channel, while one of the sequences b through e was applied to the ^{10}B channel. Broadband WALTZ-16 decoupling was applied to the ^{10}B channel during signal detection in all cases.

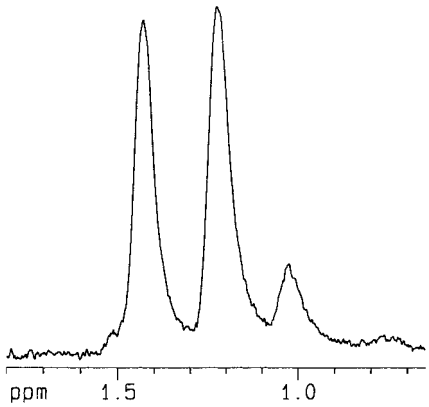

FIG. 2. ^{10}B-decoupled 400-MHz proton spectrum of BSH in D_2O, acquired in a single scan.

α, β, α', and β' is, in principle, arbitrary. However, conventionally, **A** is divided into submatrices with coherence order increasing from the upper left to the lower right ("Redfield kite"). This leads to the assignment

$$k = (S + 1 - \alpha)\delta_{\alpha\alpha'} + (3S + 2 - \alpha)\delta_{\alpha,\alpha'+1} + (5S + 1 - \alpha)\delta_{\alpha,\alpha'-1} + (7S + 2 - \alpha)\delta_{\alpha,\alpha'+2} + (8S + 2 - \alpha)\delta_{\alpha,\alpha'-2}. \quad [7a]$$

The elements of the Redfield relaxation matrix are given by

$$R_{\alpha\alpha'\beta\beta'} = \frac{1}{2}\{J_{\alpha\beta\alpha'\beta'} + J_{\beta'\alpha'\beta\alpha} - \delta_{\alpha'\beta'}\sum_{\gamma} J_{\alpha\gamma\beta\gamma} - \delta_{\alpha\beta}\sum_{\gamma} J_{\gamma\alpha'\gamma\beta'}\}, \quad [8]$$

where

$$J_{\alpha\beta\alpha'\beta'} = 2\sum_{q=-2}^{2} j_q\langle\alpha|Q_q|\beta\rangle\langle\alpha'|Q_q|\beta'\rangle, \quad [9]$$

$$j_q = \frac{C\tau_c}{1 + (q\tau_c\omega_{0S})^2}, \quad [10]$$

and

$$C = \frac{3\pi^2\chi^2(1 + \eta^2/3)}{10[S(2S - 1)]^2}. \quad [11]$$

$\chi = e^2qQ/h$ is the quadrupolar coupling constant in hertz (*1*), η is the asymmetry parameter, and τ_c is the rotational correlation time. The quadrupolar relaxation operators are given by

$$Q_0 = \frac{1}{\sqrt{6}}[3\mathbf{S}_z^2 - S(S + 1)]$$

$$Q_{\pm1} = \mp\frac{1}{2}(\mathbf{S}_z\mathbf{S}_\pm + \mathbf{S}_\pm\mathbf{S}_z)$$

$$Q_{\pm2} = \frac{1}{2}\mathbf{S}_\pm^2. \quad [12]$$

As already mentioned, in this model we are considering only the quadrupolar relaxation mechanism, and we are furthermore neglecting any coupling between the spin–lattice relaxations of spins *I* and *S* (cross relaxation). At least for the ^{1}H–^{10}B pairs in BSH, these assumptions seem to be justified by experimental observations (see below). However, the proton transverse relaxation is also affected by contributions other than the scalar relaxation contribution, and these contributions can be included by an empirical parameter, $-r_2$, which is added to the diagonal elements of the matrix **A**. The elements of the matrix **A** for $S = 3$ are listed in Tables 1 and 2. In the absence of *S*-spin irradiation, the coherences with $\Delta m_S \neq 0$ are not mixed into the observable *I*-spin magnetization, which is represented by the upper left 7×7 submatrix. Therefore, setting $\omega_2 = 2\pi\nu_2 = 0$ is equivalent to solving Eq. [6] using this 7×7 matrix (*17*). In the presence of *S*-spin irradiation, intensities are mixed between the submatrices for which the coherence orders differ by ±1. It may also be noticed that relaxation connects some of the elements within the $\Delta m_S = \pm1, \pm2$ submatrices. These terms were not included for spin 1 (*4*), but cannot be neglected if relaxation is strong enough to cause partial overlap between these coherences, for which the frequency separation is of the order of *J*.

The Redfield elements within the $\Delta m_S = 0$ submatrix represent the spin *S* spin–lattice relaxation, while the elements in the other submatrices ($\Delta m_S = \pm1$, $\Delta m_S = \pm2$) are those of spin–spin relaxation for the single-quantum and double-quantum transitions, respectively.

Equation [6] describes the density matrix evolution for the *I*-spin FID in the presence of *S*-spin decoupling. The detectable transverse magnetization in the time domain is found by

$$M_+^I(t) = \sum_{k=1}^{7} \sigma'(t). \quad [13]$$

TABLE 3
Experimental ^{10}B Spin–Lattice Relaxation Times (T_{1Q}), in ms

	In glycerol-d_8	In D_2O
320 K	4.9	
312 K	2.85	
300 K		43.5
296 K		37.4

Note. Uncertainties are estimated to be ±5%.

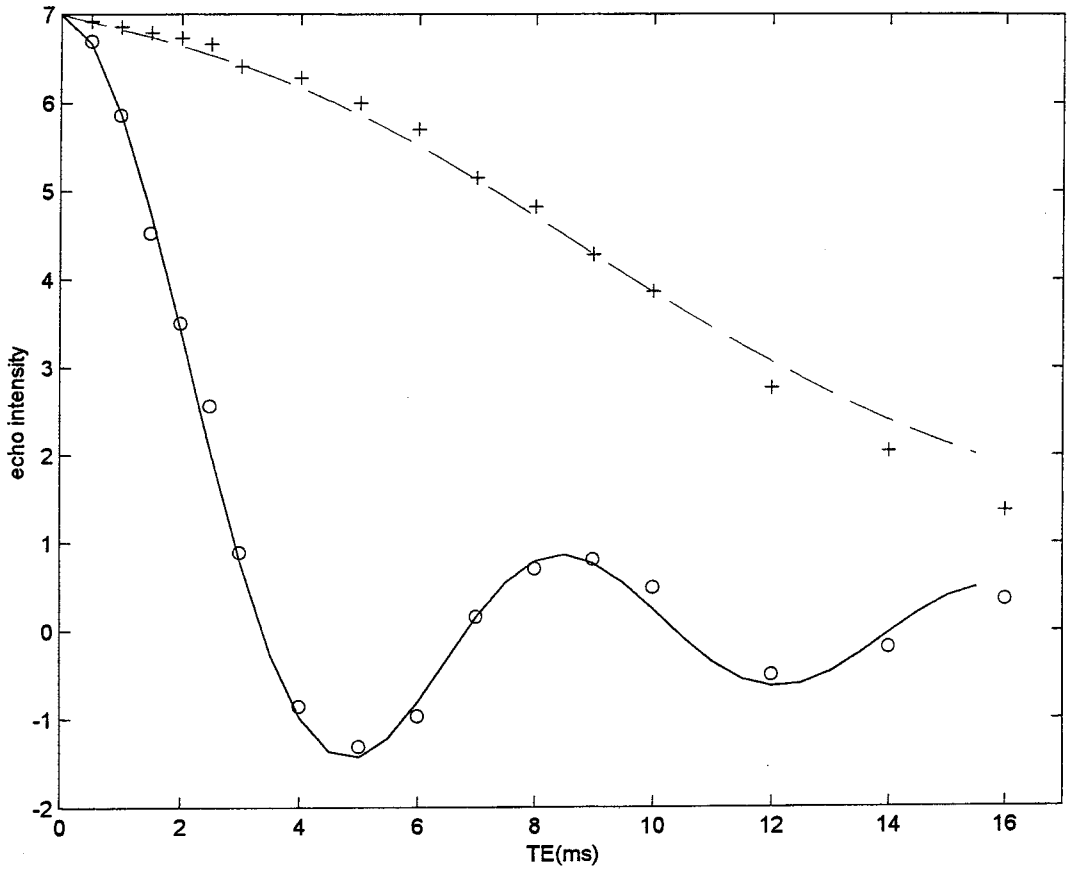

FIG. 3. Experimental results and simulated curves for ^{1}H signal decay of BSH dissolved in D_2O at 300 K, in the absence of ^{10}B irradiation. (○) Experimental points for "dual-π pulse" sequence (b). (+) Experimental points for single-π pulse sequence (d). Both simulated curves (solid line for sequence b, dashed line for sequence d) were calculated with $r_2 = 24\ s^{-1}$ and $\tau_c = 2.28 \times 10^{-11}$ s, which leads to the measured value of $T_{1Q} = 43.5$ ms.

When π pulses are applied simultaneously on both the I and S channels, the combined effects are such that the evolution described by Eq. [6] continues as if no pulses were applied, except for the influence of the resonance offset $\Delta\omega_I$, which is refocused at the time of the echo peak. Following the magnetization intensities at the echo peaks is therefore equivalent to observing an FID evolution in which the I spins are on resonance and the magnetic field is perfectly homogeneous. We shall refer to this experiment as a "dual-π pulse echo." However, when a π pulse is applied only to the I channel, the evolution leading to the echo time, $t = 2\tau$, changes to

$$\sigma'(2\tau) = e^{\mathbf{B}\tau}\mathbf{P}(\pi)e^{\mathbf{A}\tau}\sigma'(0). \qquad [14]$$

The action of the operator $\mathbf{P}(\pi)$ is to change the vector σ' into its complex conjugate. At the same time the π pulse also interchanges the spin states $\frac{1}{2}$ and $-\frac{1}{2}$ for all I spins. As a consequence, the evolution matrix changes. The new matrix, $\mathbf{B}$, is identical to $\mathbf{A}$, except that the signs of $\Delta\omega_S$ and of ω_2 are reversed. This experiment will be denoted as a "single-π pulse echo."

In the absence of irradiation, the lineshape of the spin $\frac{1}{2}$ resonance depends upon J and T_{1Q}. When $1/T_{1Q} \ll J$, the expected resolved multiplet structure will be observable, (seven lines in the case of $S = 3$), corresponding to a strongly modulated time-domain signal ("slow relaxation limit"). When $1/T_{1Q}$ is of the order of J, the proton signal will exhibit a broad, featureless lineshape, corresponding to a rapid decay of the transverse magnetization ("intermediate relaxation"). Finally, when $1/T_{1Q} \gg J$, a single narrow Lorentzian proton signal will ensue, corresponding to a single exponential decay in the time domain ("fast relaxation limit"). In this limit, the contribution of the scalar relaxation to the spin $\frac{1}{2}$ lineshape can be described by a relaxation rate given by (*1*)

$$\frac{1}{T_2^{sc}} = (2\pi J)^2 \frac{S(S+1)}{3} T_{1Q}. \qquad [15]$$

If the I spins are excited by a ($\frac{\pi}{2}$–τ–π–τ–) pulse sequence, the echo signal at 2τ will not be affected by J-coupling modulation, but will be affected by scalar relaxation. Therefore, in the slow and intermediate relaxation regimes, the single-π pulse

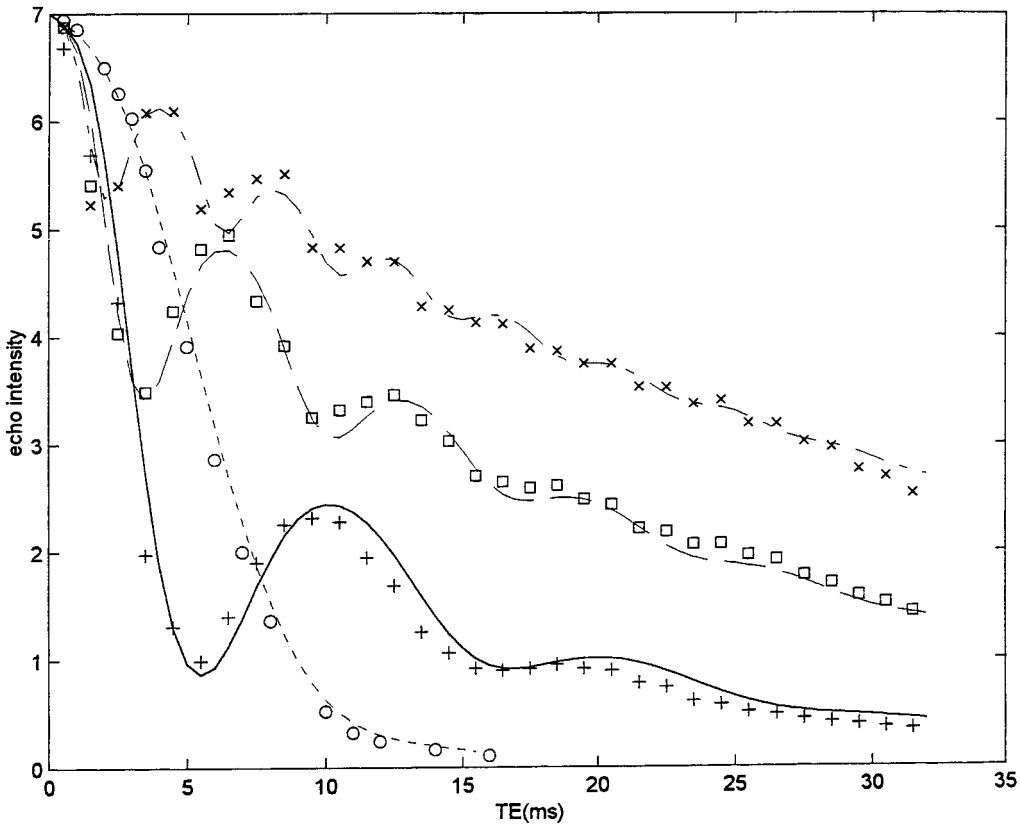

FIG. 4. Experimental results and simulated curves for ^{1}H signal decay of BSH dissolved in glycerol at 320 K. Experimental results: (○) sequence d; (+) sequence e, nominal $\nu_2 = 174$ Hz; (□) sequence e, nominal $\nu_2 = 278$ Hz; (×) sequence e, nominal $\nu_2 = 439$ Hz. All simulated curves were calculated using $\tau_c = 2.24 \times 10^{-10}$ s. Other parameters used in simulations: dotted line, $r_2 = 21.6\ s^{-1}$, $\nu_2 = 0$; solid line, $r_2 = 26\ s^{-1}$, $\nu_2 = 185$ Hz; dashed line, $r_2 = 26\ s^{-1}$, $\nu_2 = 300$ Hz; dash-dot line, $r_2 = 20\ s^{-1}$, $\nu_2 = 480$ Hz.

echo signal will be very different from the dual-π pulse signal, while the two signal types become very close, and ultimately identical, in the fast relaxation limit (*17*).

In the presence of decoupling irradiation of the *S* spins, the *I*-spin lineshape also depends upon the parameters of this irradiation, such as its strength (or amplitude), ω_2 ($=2\pi\nu_2$). If the irradiating field is strong enough to create a single Lorentzian signal for the *I*-spin magnetization, the residual linewidth of this signal (due to scalar relaxation) was predicted to obey (*3*)

$$\frac{1}{T_2^{sc}} = (2\pi J)^2 \frac{S(S+1)}{3}\left(\frac{T_{1Q}}{1+\omega_2^2 T_{1Q}T_{2Q}}\right). \qquad [16]$$

Equation [16] assumes that the *S*-spin irradiation is coherent and on resonance. If the quadrupolar relaxation is in the extreme narrowing limit, the above equation can be written as

$$\frac{1}{T_2^{sc}} = (2\pi J)^2 \frac{S(S+1)}{3}\left(\frac{T_{1Q}}{1+\omega_2^2 T_{1Q}^2}\right). \qquad [17]$$

The effect of coherent, on-resonance CW decoupling was predicted to be cyclic over a period of $1/\nu_2$, and the relative amplitudes of the resulting modulation sidebands were predicted to be of the order of $(2\pi J/\omega_2)^2$ (*10*). No detailed analysis for the behavior of single-π pulse echo signal evolution was presented so far, to the best of our knowledge, although cyclic effects in such situations were noticed for spin $\frac{1}{2}$ nuclei (*12*).

The detailed theory for quadrupolar relaxation of spin 3 was recently derived (*20*). It was shown that for the entire practically relevant range of $\omega_o\tau_c$, spin–lattice relaxation can be considered single exponential, while spin–spin relaxation is very close to single exponential for $\omega_o\tau_c$ values up to about 1.5. The relaxation rates can then be described by the analytical equations

$$\frac{1}{T_{1Q}} = 9(j_1 + 4j_2) \qquad [18]$$

$$\frac{1}{T_{2Q}} = \frac{9}{2}(3j_0 + 5j_1 + 2j_2), \qquad [19]$$

where the spectral densities j_n are defined in Eq. [10].

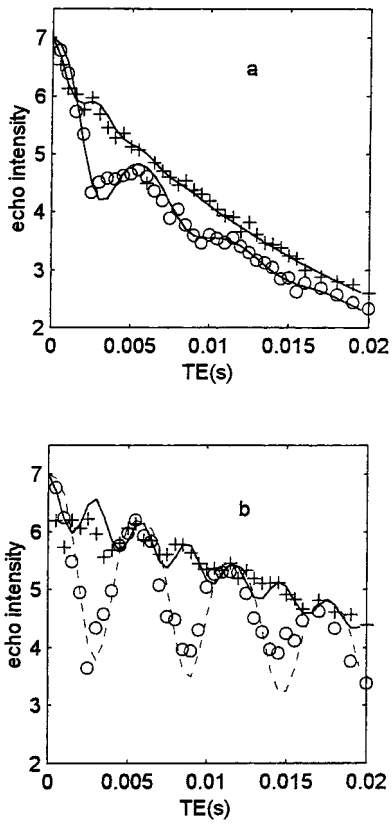

FIG. 5. Experimental results and simulated curves for ^{1}H signal decay of BSH dissolved in glycerol at 312 K (a) and D_2O at 296 K (b). All results were obtained and all curves were simulated with $\nu_2 = 340$ Hz. In both graphs the circles represent results of the single-π pulse experiment (sequence e) and the plus signs represent the results of the dual-π pulse experiment (sequence c). Further parameters used in the simulations were as follows: for BSH in glycerol (graph a), $r_2 = 25\ s^{-1}$ and $\tau_c = 4 \times 10^{-10}$ s (leading to $T_{1Q} = 2.85$ ms); for BSH in D_2O (graph b), $r_2 = 22.5\ s^{-1}$ and $\tau_c = 2.9 \times 10^{-11}$ s (leading to $T_{1Q} = 37.4$ ms).

MATERIALS AND METHODS

^{10}B-enriched BSH (≥95%) was purchased from Boron Biologicals (Raleigh, NC), and used without further purification. BSH was dissolved in D_2O, or in perdeuterated glycerol-U-d_8, 98%, Cambridge Isotope Laboratories (Cambridge, MA), at concentrations of 30–75 mM. NMR experiments were conducted on a Bruker Avance DMX-400 spectrometer (Karlsruhe, Germany), on which the ^{1}H and ^{10}B resonance frequencies were 400.1 and 43.0 MHz, respectively. A 10-mm broadband, temperature-controlled probe was used, where the ^{1}H signals were excited and detected through the outer RF coil, normally used for decoupling, and the ^{10}B resonance was irradiated via the inner observe coil.

^{1}H–{^{10}B} SEDOR experiments were conducted using the pulse sequences depicted in Fig. 1. In all experiments, sequence a was applied to the proton channel. Signal acquisition started at the echo maximum, denoted by TE. In all experiments ^{10}B broadband decoupling was applied during acquisition, using a WALTZ-16 composite pulse sequence. Sequences b and c lead to a dual-π pulse echo, and sequences d and e to a single-π pulse echo, without and with on-resonance CW ^{10}B irradiation during the echo evolution time. Signals were acquired for different values of TE, using a single scan per TE value, and were processed by Fourier transformation (FT) and phase and baseline correction. The intensity of one of the proton resonances (see Fig. 2 below) vs TE was used to characterize the time-dependent evolution of the transverse magnetization under the different conditions of sequences b through e. High-power 90° pulse lengths were about 20 μs for the ^{1}H channel and 23 μs for the ^{10}B channel. Nominal values of ν_2 for weaker power levels were found by determining the 90° pulse length (t_{90}) for direct excitation of the ^{10}B signal ($\nu_2 = 1/4t_{90}$). The values of T_{1Q} for the different solvents and temperatures were measured by inversion recovery experiments.

RESULTS AND DISCUSSION

Time Dependence of Magnetization with and without CW Irradiation

The proton spectrum of BSH dissolved in D_2O is displayed in Fig. 2, showing the signals expected for the three inequivalent proton sites in BSH at 1:5:5 intensity ratios (*20*). The peak at 1.22 ppm was used for measuring the magnetization evolution, and the center of the corresponding ^{10}B doublet (*20*) was chosen as the irradiation frequency. The coupling constant was $J = 43$ Hz, and the values of the ^{10}B spin–lattice relaxation times which were measured are listed in Table 3. In one of the cases (D_2O, 300 K), the relaxation rate was measured in the presence and absence of ^{1}H irradiation, and the results were identical, confirming that the neglect of cross relaxation is justified in our system.

Figure 3 shows some experimental results and simulations for the single-π pulse and dual-π pulse cases in which no ^{10}B irradiation is applied during the echo evolution ($\nu_2 = 0$). The pulse sequences for the ^{10}B channel therefore correspond to b and d (see Fig. 1). The simulated curves were calculated using Eqs. [6] and [14]. Apart from the independent transverse proton relaxation rate (r_2), there are no other variable parameters in the curve simulations. The values for J (43 Hz) and T_{1Q} were used as determined by independent experiments. Since T_{1Q} itself is not directly a parameter for the simulation, the value of τ_c was chosen to generate the experimental value of T_{1Q} (in this case 41 ms; see Table 3), using Eq. [18] (the Larmor frequency ω_{0S}, is of course fixed by the magnetic field strength, and $\chi\sqrt{1 + \eta^2/3}$ was set to 1.25 MHz, as determined in Ref. *20*).

The results in Fig. 3 demonstrate that, over a certain range of echo times, the signal produced by the single-π pulse sequence (d) is much stronger than that resulting from the dual-π pulse sequence (b), so that the subtraction (d − b) can be the basis

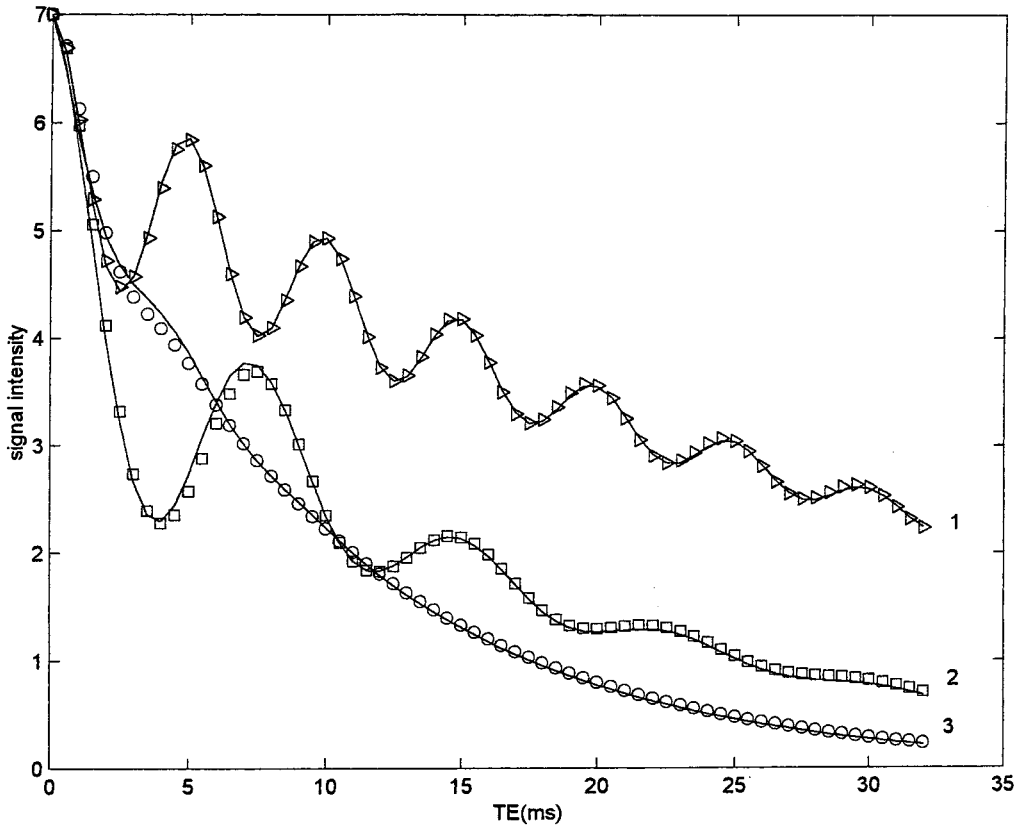

FIG. 6. The graphs in this figure show simulated behavior, which was calculated either by the full formalism for FID evolution or by Eq. [20]. Parameters used for the complete simulation: (□) $\tau_c = 1 \times 10^{-10}$ s ($T_{1Q} = 10.8$ ms), $\nu_2 = 130$ Hz; (○) $\tau_c = 6 \times 10^{-10}$ s ($T_{1Q} = 2$ ms), $\nu_2 = 200$ Hz; (△) $\tau_c = 5 \times 10^{-11}$ s ($T_{1Q} = 21.6$ ms), $\nu_2 = 200$ Hz. In all cases $r_2 = 20$ s^{-1} and $J = 43$ Hz. The solid lines show the best fits for each case, using Eq. [20] and parameters listed in Table 4.

for a sensitive inverse detection scheme (of course, for protons not coupled to ^{10}B, sequences b and d should generate identical signals). This method was indeed applied in inverse detection experiments previously reported for ^{10}B (*13*, *14*). However, it is expected that the signal difference between sequences d and b should diminish, as T_{1Q} becomes shorter (*17*). In this case, the use of continuous ^{10}B irradiation, aimed at eliminating the influence of both the *J*-coupling modulation and the scalar relaxation effects, can be expected to be the basis for a more efficient SEDOR-difference technique. Indeed, the practitioners of inverse ^{17}O detection (*18*, *19*) basically used the subtraction of scan d from scan e (single-π pulse echo without decoupling subtracted from single-π pulse echo with decoupling).

TABLE 4
Parameters Used in Simulating the Curves in Fig. 6 by Eq. [20]

	Curve 1	Curve 2	Curve 3
$\frac{A_s}{A_s + A_c}$	0.169	0.339	0.086
$\frac{\omega_2}{2\pi}$ (Hz)	200	130	200
$(r_s - r_2)^a$ (s^{-1})	54.2	121.6	352
$(r_c - r_2)^a$ (s^{-1})	8.62	40.7	85.9
$\left(\frac{1}{T_2^{sc}}\right)^b$ (s^{-1})	8.50	40.0	79.7

[a] Using $r_2 = 20$ s^{-1}.

[b] Calculated by Eq. [17], using the values of ω_2 and T_{1Q} appropriate for each curve; i.e., $T_{1Q} = 21.6$ ms for curve 1, 10.8 ms for curve 2, and 2 ms for curve 3.

At very high irradiation power levels, one should ultimately reach a situation in which the protons no longer feel the presence of attached *S* spins, in which case both sequences c and e should produce identical results, reaching the maximal possible signal level at each echo time TE. But since such power levels may be impossible to reach, particularly when using large RF coils for *in vivo* applications, we were interested in characterizing the behavior at weak to intermediate irradiation power levels. In Fig. 4, some representative results for BSH in glycerol at 320 K are displayed. These results were obtained using pulse sequence e at different power levels on the ^{10}B channel (including also the results without irradiation, i.e., sequence d). The echo peak intensities clearly display a

strong modulation with period $2/\nu_2$. The modulation depth diminishes with increasing irradiation power. In the simulated curves, the parameters were adjusted to fit the experimental value of T_{1Q}, (4.9 ms), and J was set to 43 Hz, as usual. The values for r_2 and ν_2 were adjusted to give the closest fit to the experimental results. The nominal values for ν_2 were also determined by 90° pulse measurements on the ^{10}B signal, and the best-fit values deviated from these nominal values by less than 9% (see the legend to Fig. 4). While the results are well fitted by the formal theory, some of the aspects in Fig. 4 may seem surprising. For example, for short times (before the first modulation maximum), the signal obtained in the presence of decoupling is actually weaker than the signal obtained by sequence d, without irradiation. An intuitive explanation for this phenomenon may be as follows: For weak irradiation power and short times, the entire irradiation acts like a π pulse for the S spins, in which case the single-π pulse experiment with irradiation (sequence e), actually performs like a dual-π pulse experiment without irradiation (sequence b), for which the signal is indeed weaker than that obtained with sequence d (see Fig. 3).

The observation that, for weak power levels, the use of continuous irradiation in a single-π pulse echo experiment may actually be counterproductive led us to a more careful comparison between sequences c and e, i.e., the application of continuous irradiation for dual-π pulse vs single-π pulse echoes. Representative results for this comparison are shown in Fig. 5, in which all the experiments were conducted with the same decoupling power level, and also fitted with the same value of ν_2. The results show the following: (a) The decay for the dual-π pulse echo amplitudes is modulated with period $1/\nu_2$, as predicted for an FID (*10*). (b) The modulation depth is indeed much deeper for the single-π pulse than for the dual-π pulse decay. (c) The overall decay rate (the time course through the local modulation maxima) is similar for both types of pulse sequences, and closely related to the analytically predicted value of $1/T_2^{sc}$, as will be shown below. It should also be pointed out that some experiments were conducted in which the irradiation was turned on well in advance of the initial 90° excitation pulse, and the results were identical.

Approximations by Analytical Equations

The FT of FIDs, or echo peaks obtained by dual-π pulse excitation, as shown in Fig. 5, yields spectra in which the decoupled peak has sidebands at $\pm\nu_2$. The time-domain evolution can be described by

$$M_+^I(t) = A_c\exp(-r_c t) + A_s\cos(\omega_2 t)\exp(-r_s t), \quad [20]$$

where A_c and A_s denote the centerband and sideband amplitudes, respectively, corresponding to the integrated peak areas in the FT'ed spectrum. The apparent decay rates (linewidths) of the center- and sidebands are not equal and are denoted by r_c and r_s, respectively. Figure 6 shows some examples which demonstrate the agreement between the exact simulations and Eq. [20] for a variety of conditions which are listed in detail in the legend to Fig. 6 and in Table 4. In all these cases, the spin 3 relaxation is in the extreme narrowing limit. As can be seen from comparing the values in the last two rows of Table 4, we found excellent agreement with

$$r_c = r_2 + \frac{1}{T_2^{sc}}, \quad [21]$$

where $1/T_2^{sc}$ has the value predicted by Eq. [17]. The authors of Ref. (*4*) argued that Eq. [17] rather than Eq. [16] should be used to calculate the residual scalar relaxation rate even when not in the extreme narrowing limit. However, as the results shown in Fig. 7 demonstrate, Eq. [16] seems to be correct, after all. The circular points in Fig. 7 were calculated by the exact simulation using parameters corresponding to $T_{1Q} = 1.4$ ms and $T_{2Q} = 0.411$ ms ($\omega_o\tau_c = 1.5$). The curves were calculated according to a simple exponential decay, using the decay rate as expressed in Eq. [21], and calculating $1/T_2^{sc}$ either by Eq. [16] (solid curve) or by Eq. [17] (dashed curve). Equation [16] clearly provides a better approximation to the exact simulation, which is not too surprising, in view of the fact that the evolution matrix **A** (Table 1) contains the spectral densities j_0, which contribute to T_{2Q} but not to T_{1Q}.

In general, the modulation (or sideband intensity) will be prominent if the lineshape in the absence of decoupling is in the slow to intermediate relaxation regime, i.e., for $2\pi JT_{1Q} \geq 1$. The relative intensities of the modulated component are of the order of $(J/\nu_2)^2$. The apparent decay time of the modulated components $(1/r_s)$ is approximately equal to the time over which J-coupling modulations can be observed in the nondecoupled FID. As T_{1Q} becomes shorter and the relaxation is in the fast limit, the modulations caused by weak irradiation will be quenched, both by decrease of A_s and by increase of r_s.

The above description applies to the dual-π pulse echo signal. As apparent in Fig. 5, the modulation of the single-π pulse echo signals is much more prominent, with both larger amplitudes and slower decay rates of the modulated component. A description by Eq. [20] is still possible (with ω_2 replaced by $\omega_2/2$) and approximates the exactly simulated (or experimental) data well, although not as accurately as for the dual-π pulse case. In the cases which we examined, either experimentally or by simulations, it was found that there was close agreement between the values of r_c found by fitting the data to Eq. [20], and $1/T_2^{sc}$ calculated by Eq. [16], for low values of $1/T_2^{sc}$, but that deviations of up to 50% were observed when $1/T_2^{sc}$ reached values of the order of 10^2 s^{-1} (corresponding to $\omega_2^2 T_{1Q} \approx 3 \times 10^3$).

Decoupling by Composite Pulse Sequences (CPD)

Under certain experimental conditions, decoupling by CW irradiation may not be satisfactory, if a range of ω_{oS} frequen-

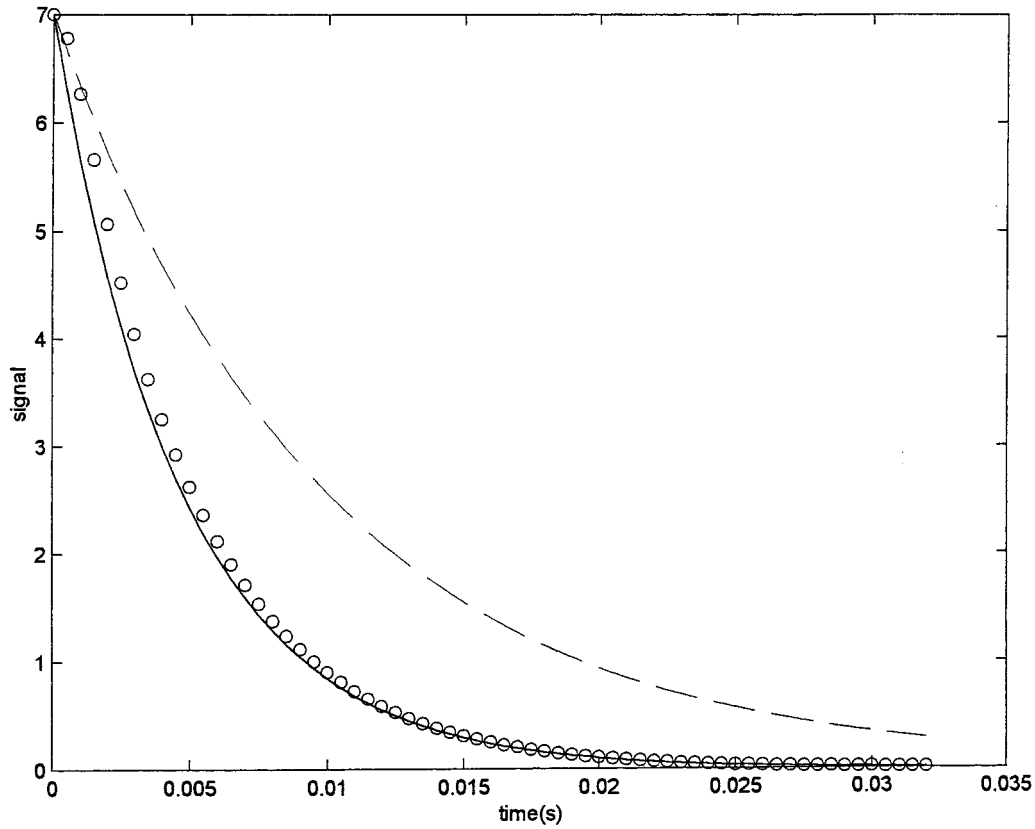

FIG. 7. Circles were calculated by complete simulation, using $\tau_c = 5.55 \times 10^{-9}$ s, which corresponds to $T_{1Q} = 1.4$ ms, $T_{2Q} = 0.41$ ms, and $\nu_2 = 200$ Hz. The solid line was calculated by Eq. [16] ($1/T_2^{sc} = 212\ s^{-1}$) and the dashed line by Eq. [17] ($1/T_2^{sc} = 100.6\ s^{-1}$).

cies must be covered. Such a situation may arise, for example, if field gradients are applied during the echo evolution. We therefore examined the echo amplitude evolutions in single-π pulse experiments, using three different CPD schemes and irradiation levels for which $\omega_2^2 T_{1Q}^2 \gg 1$. Only on-resonance irradiation is considered, to allow a direct comparison with CW irradiation. The off-resonance behavior for different broadband decoupling schemes was recently evaluated for $S = 1$ (*21*). The CPD sequences consisted of a modified MLEV-4 pulse train ($RRRR$), in which a simple 180° pulse was used as inversion element R (*22*), as well as WALTZ-4 and WALTZ-16 sequences (*23*). The results are summarized in Fig. 8 and Table 5. In Fig. 8, the apparent decay rates of the echo peaks are plotted as a function of $1/\omega_2^2$, for which a linear relation is predicted by Eq. [17], if $\omega_2^2 T_{1Q}^2 \gg 1$. In this set of experiments, the irradiation power was sufficiently high to justify this approximation, and also suppress the modulation effects, so that decay rates could be measured by simple single exponential fits. In analogy to Eq. [17], we can define an empirical relation:

$$\frac{1}{T_2} = r_2 + \frac{(2\pi J)^2}{3} \frac{S(S+1)}{T_{1Q}} \frac{1}{\beta \omega_2^2}. \qquad [22]$$

TABLE 5

Parameters Relating the Residual Transverse Decay Rates to Applied Irradiation Power for Different CPD Methods, According to Eq. [21], Applied to BSH in Glycerol at 320 K

CPD	r_2 (s^{-1})	β
MLEV-4	32.1	0.95
WALTZ-4	24.6	0.61
WALTZ-16	22.2	0.50

Table 5 lists the intercepts and values of the constant β derived from the slopes of the linear fits shown in Fig. 8. One should recall that for the same sample and temperature, the CW irradiation results could be fitted to theory using r_2 values of about $24 \pm 2\ s^{-1}$, and $\beta = 1$ (see Fig. 4 for representative results). Thus, it appears that the WALTZ-4 and WALTZ-16 sequences are less efficient than on-resonance CW irradiation at the same power level, since their values of β are smaller than unity. Moreover, one can detect a trend showing a decrease in β which is commensurate with the increase in the length of the effective unit inversion element in the CPD sequence. The MLEV-4 sequence with

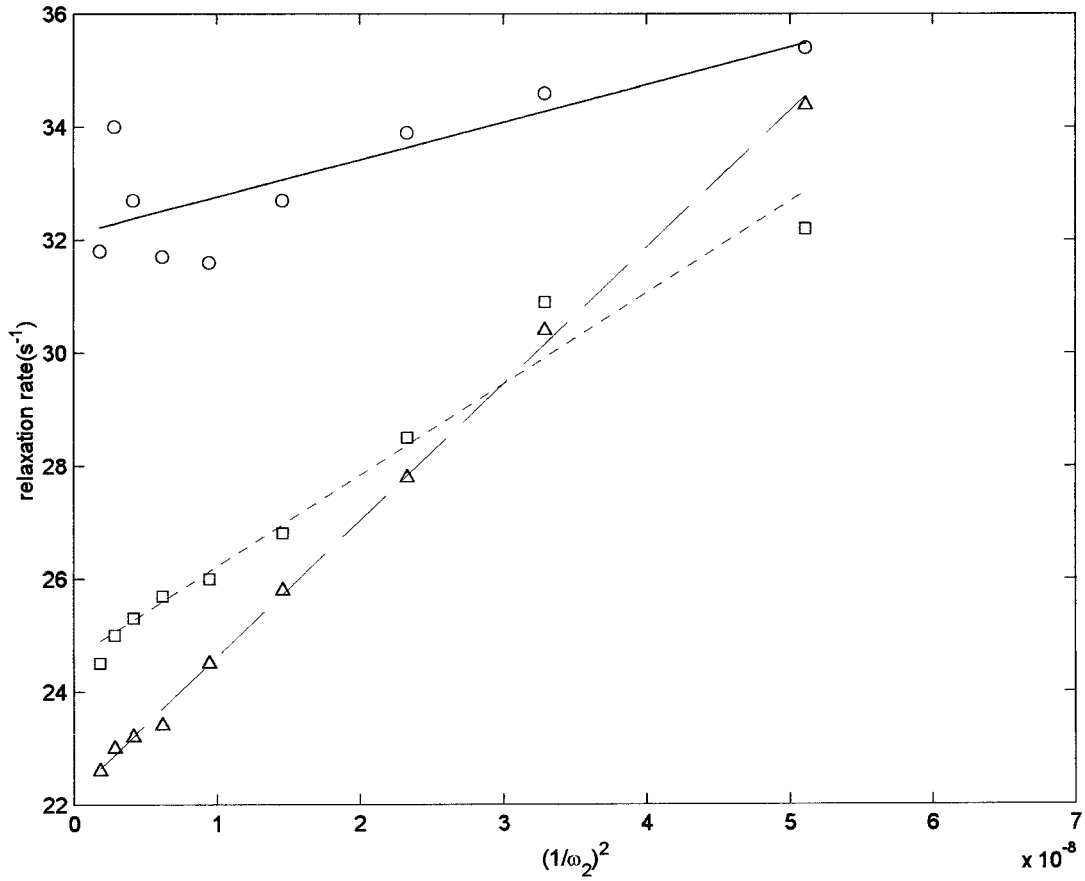

FIG. 8. Single exponential relaxation rates derived from SEDOR experiments (sequence e), using CPD at different power levels during echo evolution, conducted on BSH in glycerol at 320 K. (○) 180–180–180–180; (□) WALTZ-4; (△) WALTZ-16. The straight lines were calculated using Eq. [22], $J = 43$ Hz, $T_{1Q} = 4.9$ ms, and parameters listed in Table 5.

$R = 180°$ uses the shortest possible inversion element and achieves approximately the same efficiency as CW irradiation. However, it is also evident from the results in Fig. 8 and Table 5 that the more elaborate decoupling schemes WALTZ-4 and WALTZ-16 achieve an overall better performance at the higher power levels, because the intercept in the fit to Eq. [22] for these sequences (r_2) is lower. We tentatively interpret these differences in the intercept to reflect the varying sensitivities of the different CPD sequences to spatial inhomogeneities in the decoupling field, since the order of decrease in r_2 is commensurate with the expected increase in robustness to variations in ω_2.

In summary, the effects of irradiating a quadrupolar spin $S = 3$ (^{10}B), coupled to spin $I = \frac{1}{2}$ (^{1}H), on the FID and spin-echo evolution of the proton magnetization were observed and fully accounted for by theoretical simulations, which calculated the density matrix evolution under the Redfield superoperator. The experimental goal of such irradiation is to achieve a transverse decay of the I-spin magnetization at the limiting rate which would be obtained if the attached S spins were absent. When the irradiation is not strong enough to accomplish this goal, the I magnetization signal is modulated and decays more rapidly than the limiting rate. The modulation frequency and depth, and the residual contribution of the scalar relaxation, depend upon the coupling constant, the irradiation power, and the quadrupolar relaxation time of the S spins. The modulation is much more prominent for proton spin echoes than for continuous FID evolution (or "dual-π pulse" echoes).

There may be some practical conclusions from this work, concerning the experimental implementation of pulse sequences aimed at selective, spatially resolved detection of protons which are coupled to quadrupolar nuclei. Such sequences are often based on the subtraction of "low-intensity" scans, in which the S-coupled protons have minimal signal, from "high-intensity" scans, in which they have maximal signal. S-spin irradiation will be used to generate the signal for the high-intensity scans. This paper provides the means for planning the optimal parameters for such sequences, particularly the echo time TE. Even when the irradiation power is not

strong enough, the adverse effect from the cyclic modulation can be avoided by choosing TE to coincide with the predicted modulation peaks.

ACKNOWLEDGMENT

This research was supported by a grant from the G.I.F., the German–Israeli Foundation for Scientific Research and Development.

REFERENCES

1. A. Abragam, "Principles of Nuclear Magnetism," Oxford Science, New York (1989).
2. J. M. Anderson and J. D. Baldeschwieler, Nuclear magnetic double resonance spectrum of ammonia, *J. Chem. Phys.* **40,** 3241–3248 (1964).
3. D. T. Browne, G. L. Kenyon, E. L. Packer, H. Sternlicht, and D. M. Wilson, Studies of macromolecular structure by ^{13}C nuclear magnetic resonance. II. A specific labeling approach to the study of histidine residues in proteins, *J. Am. Chem. Soc.* **95,** 1316–1323 (1973).
4. N. Murali and B. D. N. Rao, Lineshape variations of a spin $\frac{1}{2}$ nucleus coupled to a quadrupolar spin subjected to RF irradiation, *J. Magn. Reson. A* **118,** 202–213 (1996).
5. N. R. Skrynnikov, S. F. Lienin, R. Brüschweiler, and R. R. Ernst, Efficient scalar spin relaxation in the rotating frame for matched radio-frequency fields, *J. Chem. Phys.* **108,** 7662–7669 (1998).
6. Ē. Kupče, Effect of sweep direction on sidebands in adiabatic decoupling, *J. Magn. Reson.* **129,** 219–221 (1997).
7. M. R. Bendall and T. E. Skinner, Coherence sidebands in adiabatic decoupling, *J. Magn. Reson.* **129,** 30–34 (1997).
8. A. J. Shaka, P. A. Barker, C. J. Bauer, and R. Freeman, Cyclic sidebands in broadband decoupling, *J. Magn. Reson.* **67,** 396–401 (1986).
9. W. A. Anderson and R. Freeman, Influence of a second radiofrequency field on high-resolution nuclear magnetic resonance spectra, *J. Chem. Phys.* **37,** 85–103 (1962).
10. J. S. Waugh, Theory of broadband spin decoupling, *J. Magn. Reson.* **50,** 30–49 (1982).
11. A. J. Shaka and J. Keeler, Broadband spin decoupling in isotropic liquids, *Prog. NMR Spectrosc.* **19,** 47–129 (1987).
12. R. Freeman and H. D. W. Hill, Determination of spin–spin relaxation times in high-resolution NMR, *in* "Dynamic Nuclear Magnetic Resonance Spectroscopy" (L. M. Jackman and F. A. Cotton, Eds.), pp. 131–162, Academic Press, New York (1975).
13. F. De Luca, R. Campanella, A. Bifone, and B. Maraviglia, Boron-10 double resonance spatial NMR detection, *Chem. Phys. Lett.* **186,** 303–306 (1991).
14. P. Bendel, J. Zilberstein, and Y. Salomon, *In-vivo* detection of a boron neutron capture agent in melanoma by proton observed ^{1}H–^{10}B double resonance, *Magn. Reson. Med.* **32,** 170–174 (1994).
15. P. Kinesh, E. W. Randall, and S. C. R. Williams, SEDOR indirect imaging. ^{14}N and ^{15}N imaged by *J*-modulation techniques, *J. Magn. Reson. B* **105,** 253–255 (1994).
16. C. P. Slichter, "Principles of Magnetic Resonance," Springer-Verlag, Berlin (1990).
17. P. Bendel, Lineshape and relaxation of spins $I = \frac{1}{2}$ coupled to $S = 3$. Application to selective detection of protons attached to boron-10, *J. Magn. Reson. A* **117,** 143–149 (1995).
18. I. Ronen and G. Navon, A new method for proton detection of H_2 ^{17}O with potential applications for functional MRI, *Magn. Reson. Med.* **32,** 789–793 (1994).
19. A. H. Stolpen, R. Reddy, and J. S. Leigh, ^{17}O-decoupled proton MR spectroscopy and imaging in a tissue model, *J. Magn. Reson.* **125,** 1–7 (1997).
20. A. Baram and P. Bendel, Quadrupolar relaxation of spin 3 in the intermediate $\omega_o\tau_c$ regime, *J. Magn. Reson.* **129,** 10–18 (1997).
21. S. A. Smith and N. Murali, Relaxation effects in a system of a spin-1/2 nucleus coupled to a quadrupolar spin subjected to rf irradiation: Evaluation of broadband decoupling schemes, *J. Magn. Reson.* **136,** 27–36 (1999).
22. M. H. Levitt and R. Freeman, Composite pulse decoupling, *J. Magn. Reson.* **43,** 502–507 (1981).
23. A. J. Shaka, J. Keeler, T. Frenkiel, and R. Freeman, An improved sequence for broadband decoupling: WALTZ-16, *J. Magn. Reson.* **52,** 335–338 (1983).